Machinability and grindability of high-carbon tool steel manufactured by powder bed fusion electron beam

(article starts on next page)

Available online at www.sciencedirect.com

ScienceDirect

Procedia CIRP 141 (2026) 262–267

www.elsevier.com/locate/procedia

10th Conference on High Performance Cutting (CIRP-HPC 2026)

Machinability and grindability of high-carbon tool steel manufactured by powder bed fusion electron beam

Seyed B. Hosseini[a]*, Tomas Gustavsson[a], Jonathan Ekdahl[b], Petrus Dahlqvist[b], Daniel N.-Jansson[a], Amir Malakizadi[b, c]

[a]*AB SKF, SE-415-50, Gothenburg, Sweden*
[b]*Division of Materials and Manufacture, Department of Industrial and Materials Science, Chalmers University of Technology, Gothenburg, SE-412 96, Sweden*
[c]*inspire AG, Technoparkstrasse 1, Zürich 8005, Switzerland*

* Corresponding author. Tel.: +46-70-282 2515; *E-mail address:* seyed.hosseini@skf.com

Abstract

Additive manufacturing (AM) enables the production of complex near-net-shaped components; however, limitations in surface integrity and dimensional accuracy often necessitate post-processing such as heat treatment and machining to achieve functional performance. This study investigates the machinability and grindability of Vibenite® 280, a high-speed tool steel manufactured using Powder Bed Fusion–Electron Beam (PBF-EB) process. In the hot-isostatic-pressed (HIPed) and heat-treated condition, Vibenite® 280 exhibits a hardness of ~68 HRC (930 HV1) and its microstructure containing ~20 vol.% V-, Mo-, and W-rich carbides, posing significant challenges for precision finishing. Grinding trials using Al_2O_3 and cubic boron nitride (CBN) wheels demonstrated that CBN provided superior process stability, thermal robustness, and surface integrity, achieving a R_a ~0.3 µm and high G-ratios without thermal damage, even at elevated specific grinding energies. However, the poor as-built surface quality and dimensional deviations required a pre-grinding step prior to finishing. Hard turning tests revealed that coated cemented carbide inserts offered the best compromise between tool wear and surface finish, though chipping and accelerated wear at higher feeds remained problematic. Residual stress analysis indicated beneficial compressive states with a characteristic hook-shaped profile after hard turning, supporting improved fatigue performance. Overall, the findings confirm the feasibility of precision machining Vibenite® 280 in its hardened condition, enabling its application in demanding environments requiring exceptional wear resistance and dimensional accuracy.

Keywords: Additive Manufacturing; Powder Bed Fusion Electron Beam Melting; Hard Turning; Grinding; Surface Integrity

1. Introduction

The superior properties of high-speed steels (HSS) render them viable replacements for conventional steel grades used in high-performance bearing applications subjected to severe tribological conditions. Such steels are a subset of high-carbon tool steels that contain a significant amount of tungsten and other elements like chromium, vanadium and cobalt to improve their high temperature hardness and wear resistance [1]. Normally such steel grades are processed using casting [2], electroslag remelting [3], and powder metallurgy [4]. The advancement of additive manufacturing (AM) has recently enabled manufacturing of HSS components with complicated geometry and near-net-shape [5]. Various AM techniques, such as powder bed fusion, direct energy deposition and metal binder jetting have been widely studied. These methods are applied in demanding sectors such as aerospace and medical. Powder bed fusion (PBF) process using either a laser (PBF-LB) or an electron beam (PBF-EB) as energy sources are the most widely used technologies in the industry. These methods produce

10.1016/j.procir.2026.03.068

dense parts with near-net accuracy and reproducibility. They also offer good mechanical and thermal properties, allowing precise control of the microstructure during printing [6-7]. In particular, the elevated processing temperatures in PBF-EB enable the defect-free fabrication of tool [8] and high-speed steels [9, 10], effectively mitigating their inherent susceptibility to hot-tearing, cold-cracking, and the formation of brittle carbide networks. The processibility and tribological properties of additively manufactured tool steels have been investigated in several studies. For example, Iakovakis et al. [9] studied the tribological performance of carbide rich tool steels, Vibenite® 150, 280 and 290 manufactured with PBF-EB. The authors reported that Vibenite® 280 had the best wear performance and lowest coefficient of friction (CoF) amongst the different Vibenite® grades and compared to those of AISI 52100 steel – an industry-standard bearing steel. Arumskog et al. [10] demonstrated how to control the carbide size in the high-carbon Fe- and Co- alloys focusing on the Vibenite® 150, 280, 290 and 480. The authors demonstrated how the carbide size can be controlled by controlling the volumetric energy density (VED), i.e. higher VED results in larger carbides. In agreement with Iakovakis et al. [9], Arumskog et al. [10] reported that Vibenite® 280 exhibited superior abrasive wear properties compared to AISI 52100 steel. This performance was attributed to coarse carbides acting as the primary load carrying phase. Nevertheless, the assessment of machinability constitutes a pivotal criterion for evaluating the feasibility of replacing the conventional steels with these advanced alloys, as it validates that requisite dimensional tolerances and surface specifications can be achieved with minimum comparable or even better manufacturing efficiency. Prior investigations have addressed the machinability of these AM alloys marginally. For example, Franklin et al. [11] investigated the grindability of Vibenite® 150, 290 and 480 alloys. The authors reported that employing a grinding wheel with an open bond and with CBN abrasives is suitable for such ultra-hard AM materials. They further recommended that grinding process should be carried out in two steps due to the initial high roughness of as-printed surfaces. Moreover, depending on the carbide morphology (size, shape, volume fraction and type) grinding parameters should be carefully adjusted. This is in line with the investigations on conventional (cast) tools and high-speed steels. For example, Tarasov [12, 13], and Roberts [14] reported that Vanadium (V) content had major contribution to the grindability of such steel. When studying the G-ratio (volumetric ratio between removed material over consumed grinding wheel) versus Equivalent Carbide Content, ECC, [15] (eq. 1), König and Messer [16] observed a trend in reduced G-ratio with increasing ECC. Badger [17] reported on the grindability of HSS by measuring the G-ratio and power consumption in surface grinding. He reported that the dominant factor affecting the grindability, was the size of the V-carbides.

$$ECC\ (\%) = W + 1.9 * Mo + 6.3 * V \qquad \text{(eq.1)}$$

where W, Mo, V are the % composition of tungsten, molybdenum and vanadium, respectively in the alloy. Considering eq.1, it can be determined that the ECC for AISI 52100 steel, M2, M50 and Vibenite® 280 are 0 %, 28 %, 15 % and 60 % respectively. This will have a significant impact on the machinability of the alloy. Indeed, AM provides an unprecedented opportunity to process HSS produced near-net-shape with complex geometries. However, it also brings substantial challenges forward with respect to machining, especially when it comes to ultra-hard materials like Vibenite® with respect to its carbide morphology. These characteristics in combination with the rough as-printed surfaces have a detrimental effect on the cutting tool and grinding wheels. There is a major gap in cost-effective methods for processing of additively manufactured components while preserving bearing quality. This study explores the machinability and grindability of ultra-hard Vibenite® 280.

2. Experimental work

2.1. Materials and AM process

The printed parts were supplied by VBN Components AB, Sweden. The chemical composition and the hardness in the hot isostatic press (HIP) and heat-treated condition is shown in Table 1. Details about the HIP and heat treatment cycles for the Vibenite® 280 material can be found in Ref. [18]. The feedstock used in the PBF-EB process was a gas-atomized, pre-alloyed powder supplied with a nominal sieve classification of 50–150 µm. According to the supplier, the majority of particles are concentrated near ~125 µm [10]. The carbide content of the alloy is estimated to be ~20 vol.% [10]. To investigate the machinability of Vibenite® 280, ring-shaped specimens according to Figure 1 were fabricated using the PBF-EB process in a Colibrium A2X system. Finishing operations, grinding and hard turning, were performed only on the outer diameter. The radial machining allowance was 0.6 mm, yielding a final specified outer diameter of 57.6 mm. Prior machining face-ground were done for all specimens [19].

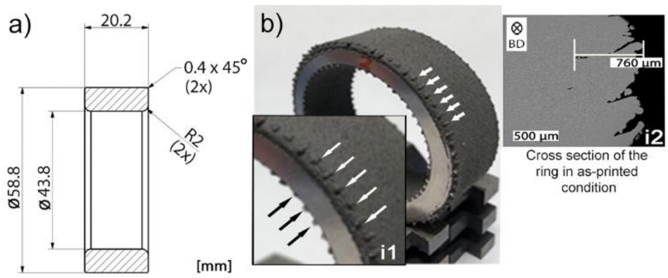

Figure 1. a) Geometry and principal dimensions of the additively manufactured ring. (b) As-printed rings with surface undulations along the build direction (arrows); inset (i1) shows a detailed view. (i2) Cross-section indicating a surface irregularity height of ~760 µm relative to the build direction (BD) parallel to axial direction.

The build chamber was 200×200×380 mm^3 and the scanning direction was rotated by 90° for each layer. The beam acceleration voltage was constant at 60 kV, the beam power was set to 720 W, and the layer thickness was 160 µm. The beam current was 12 mA and the line offset was 0.2 mm. A preheating temperature of ~900 °C was throughout the printing. The process was conducted under a standard PBF-EB atmosphere, with the chamber vacuum maintained and periodically purged with small amounts of helium, consistent with standard operating condition for Colibrium EBM systems.

Table 1. Chemical composition of Vibenite 280® alloy in wt% and hardness [10]. The alloy is patent protected.

Material	C	Cr	Mo	W	V	Co	Fe	Hardness
V280®	2.3	4.2	7.0	6.5	6.5	10.5	Bal.	933 HV1

2.2. Grinding

Grinding assessments were conducted on an SGP320 machine (UVA Lidköping) using shoe centerless work holding, where the ring is supported by two shoes and a driven datum plane [20]. Rotational stability depends on the offset between the datum plane axis and the workpiece center of gravity and the out-roundness of the ring. As material is removed, the center of gravity shifts and hence the rotational stability, limiting the maximum removable allowance, based on used eccentricity offset, and initial out of roundness. The grindability study followed the SKF wheel test method [21]. Four specific removal rates (Q'_w) were applied with a 1 s dwell time on pre ground rings. Each feed rate was tested over two dress intervals with five rings per interval. The specific material removal was 44.8 mm³/mm (ΔØ = 0.5 mm) per ring. Wheel speed was v_s = 60 m/s and ring speed v_w = 1.9 m/s. Spindle power, dimensional variation, and surface roughness were evaluated. Dressing was performed using a rotary diamond disc (tip radius 1 mm, using a dress overlap ratio of 10.4), targeting R_a = 0.3 µm. AM rings exhibited larger diameter variation, out of roundness, and surface roughness than conventional rings. Initial ovality was Δ Ø ~0.4 mm and the arithmetical mean height, Sa, of the as-printed surfaces was ~55 µm. A pre grinding step at reduced ring speed (v_w = 1 m/s, Q'_w = 4 mm³/mm·s) was therefore introduced to reach Ø = 58.3 mm, followed by a second step to Ø = 57.8 mm for grindability testing. Diameter variation (~0.6 mm) and ovality (~0.2 mm) were measured using an acoustic emission touch detector (Accretech SBS SB5500 with exact control), presented in Table 2. Grindability tests were first performed on rings from Ø 57.8 to 57.3 mm (suffix "_1") using Al_2O_3_1 and CBN_1 wheels. For Al_2O_3_1, dress compensation was 20 µm with Q'_w= 0.8–6 mm³/mm·s. For CBN_1, dress compensation was 2 µm with Q'_w = 2.4–10 mm³/mm·s. Loss of dress contact and excessive wheel wear at a Q'_w=10 mm³/mm·s required a second assessment on rings from Ø 57.3 to 56.8 mm (suffix "_2"). Al_2O_3_2 used unchanged settings, while CBN_2 employed 4 µm dress compensation and removal rates matching those of Al_2O_3. Based on the material composition, rapid wheel wear was expected, making surface integrity assessment essential. Residual stresses were measured, and the maximum surface temperature was estimated using Eq. (2). During shallow cut grinding, approximately 85% of the heat enters the workpiece for Al_2O_3 wheels and 45% for CBN wheels [22], reflecting the higher thermal conductivity of CBN. In eq.2 heat flux q expressed in W/m² index w, means the heat flux entering the work piece. The thermal parameter β_w was calculated as 11 520 J·m⁻²·K·s⁰·⁵ for ASP2060 at 1100 K. As real contact length is not known, geometrical contact length (l_g) is used.

$$T_{max} = \frac{q_w}{\beta_w}\sqrt{\frac{l_g}{v_w}} \quad \text{(eq.2)}$$

Table 2. Variation in incoming size and ovality, 75th and 25th percentiles.

	Max	75th	Mean	25th	Min
ΔØ to remove in mm	1.05	0.76	0.72	0.64	0.48
ΔØ ovality in mm	0.31	0.24	0.20	0.17	0.11

2.3. Hard turning

Prior to select the appropriate tool grades and machining condition, several screening tests were conducted using various CBN, ceramic and coated cemented carbide tools as published in Ref. [19]. The results showed that the utilization of coated cemented carbide represented an optimal trade-off concerning tooling costs, surface integrity, and dimensional accuracy and will be presented here in detail. The hard turning tests were performed on an EMCO TURN 365 CNC lathe. The cutting speeds used were 40, 60 and 80 m/min and following feeds were 0.05, 0.10 and 0.15 mm/rev. The depth of cut was kept constant at 0.1 mm throughout all tests. Three types of cutting inserts were used: the PVD-coated CNMG120408-SF 1205 (Sandvik Coromant), and the PVD-coated CNM120408-MF1 TH1000 and TS2000 (Seco Tools). The 1205 grade featured a PVD AlTiN coating, while the Seco Tools TH1000 and TS200 grades were PVD-coated with a TiSiN–TiAlN nanolaminate, and TiAlN+TiN, respectively. Cutting edge radii were measured using a GFM MikroCAD+ system, and inserts with comparable edge radii were selected for testing: 23.5 ± 2.5 µm (SF 1205), 27.5 ± 2.5 µm (TH1000), and 32.5 ± 2.5 µm (TS2000). For all tests the CoroTurn HP PCLNL2525M 12HP tool holder were used. The coolant (8.0–8.4% emulsion, 6–8 bar inlet pressure) was supplied on the rake side. Cutting forces were recorded using a Kistler 9257A three-component dynamometer. To avoid clamping the rings, a specially designed pallet combined with an internal gluing procedure was used. The gluing process was optimized iteratively: rings were bonded and cured for different intervals, then pushed laterally into a turning machine while the detachment force was measured using the dynamometer.

Since the actual turning forces were not known beforehand, no specific force threshold could be defined. Instead, the process was refined until the required detachment force was ~3000 N, significantly higher than the forces encountered during turning. Due to the surface roughness and large diametral variations in the as-printed condition, also the hard-turning tests was done in two stages (P1 and P2), each with five passes. P1 targeted a diameter of 58 mm and P2 targeted a diameter of 57 mm. For each stage a fresh cutting edge was used to monitor wear consistently. The surface irregularities and diameter differences in P1 made cutting-force measurements unreliable, so only the P2 forces are reported.

2.4. Material characterization

Surface roughness was characterized using laser confocal microscopy (Olympus LEXT 5000) and a stylus profilometer (Taylor Hobson Form Talysurf) with a 2 µm radius conisphere tip. The confocal system provides 0.4 µm lateral resolution and stitched areal maps, making it suitable for the as-printed PBF-EB surfaces, which were evaluated over 2566 × 2562 µm using

S and L filter cutoffs of 8 µm and 250 µm. To ensure cross method comparability, the machined surfaces were also measured once with the confocal system over 1078 × 1080 µm with 0.8 µm and 250 µm cutoffs. For the full set of as-machined specimens, routine roughness values (R_a) were obtained using the Form Talysurf with a 250 µm cutoff in accordance with ISO profile standards. This combined approach ensures accurate areal capture of the rough as-printed surfaces while providing standardized, ISO compliant R_a measurements for the machined condition. Residual stresses were measured using X-ray diffraction with a G2R XStress 3000 system (Stresstech Oy) equipped with a chromium source. A modified $\sin^2\psi$ method was applied using five tilt angles in each direction (±45°), totaling ten measurements. Analysis focused on the (211) lattice plane at a diffraction angle of 156.4°. Stresses were calculated assuming elastic behavior per Hooke's law, with a Young's modulus of 211 GPa and a Poisson's ratio of 0.3. Sub surface residual stresses were obtained by electrochemical etching in a 3 M NaCl solution at a constant 0.2 A. Each 50 s etching cycle removed approximately 25 µm, and cycles were repeated to reach the required depth. The bulk microstructure and machined cross-sections were examined using light optical microscopy and a TESCAN scanning electron microscope equipped with EDX and EBSD detectors.

3. Results and discussions

3.1. Grinding

The objective was to evaluate the performance of Al_2O_3 and CBN wheels when grinding Vibenite® 280. The wheels were dressed to target a surface roughness of R_a ~ 0.3 µm, which was achieved in the CBN_2 series. The ground roughness depends on both wheel topography, accumulated material removed since the dressing and the removal rate. Figure 2 shows the change in surface roughness between the 1st (44.8 mm^3/mm removed since dressing) and 5th (224 mm^3/mm removed since dressing) rings within each dressing interval at different removal rates. The 5th ring in each interval is marked with suffix "$_e$" while the first ring is without any suffix. CBN_2 have the finest roughness and just a small increase from the 1st to the 5th ring. Hence, it is fair to use the CBN_2 as a reference for how an as dressed topography should behave. For Al_2O_3, no significant difference was observed between the first "_1" and second "_2" attempts; and the data were therefore combined.

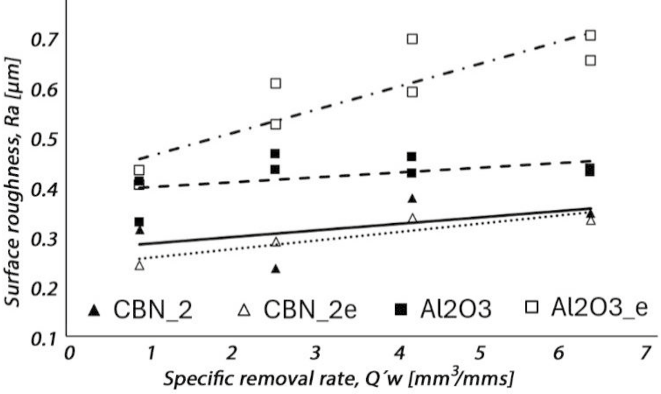

Figure 2. Surface roughness after 1st and 5th ring in the dress intervals for the CBN_2 and the Al_2O_3 wheel tests.

Notably, for Al_2O_3 already the 1st ring exhibited high roughness, which increased to R_a ~0.6 µm at the 5th ring for the higher feeds indicating a rapidly degraded wheel topography. Furthermore, the specific grinding energy increased from 1st to 5th ring. Figure 3 show data for the 5th ring. The energy increase, directly from grinding power, indicate that the normal force between ring and wheel increases. Hence resulting in increased elastic deflection during grinding, giving oversized ground rings. Overall, Al_2O_3 does not provide a robust process for precision grinding of Vibenite® 280. For CBN_1 and CBN_2, the specific grinding energy were stable in each dress interval, although being higher for the 1st ring as compared to the 2nd through to the 5th ring. For CBN_1, dressing contact (AE-supervised) was lost at $Q'_w \geq 4$ mm³/mm·s, although roughness, power, and size variation remained stable. At the highest feed rate (Q'_w = 10 mm³/mm·s), wheel wear became excessive. The process remained stable up to 6 mm³/mm·s, suggesting that the behavior is governed by intrinsic wheel properties rather than forced conditions. Allowing a roughness of R_a ~ 0.45 µm resulted in excellent size control and a significantly higher G ratio. Consequently, CBN_1 data were included in the specific grinding energy and thermal analysis (Figure 3) but excluded from the roughness discussion in Figure 2. CBN_2 was evaluated at lower Q'_w (0.8–6 mm³/mm·s) with increased dress compensation. This enabled achieving R_a ~ 0.3 µm with robust and stable process performance. Figure 3 presents specific grinding energy, normalized to grinding AISI 52100 at 6 mm³/mm·s and R_a ~ 0.45 µm. For Vibenite® 280, the specific energy was approximately twice as high for CBN_1 and three times higher for Al_2O_3. This is attributed to the high carbide content of Vibenite® 280, which rapidly dulls Al_2O_3 abrasives. CBN grains, being harder, can cut through carbides and maintain sharpness longer, resulting in improved robustness and surface quality. The T_{max} from Eq.2 was presented in Figure 3, normalized to the highest feed rate of the Al_2O_3 wheel, shows that CBN_2 achieved a finer surface with approximately 50 % lower thermal load. Allowing higher roughness (CBN_1) further reduces the thermal stress.

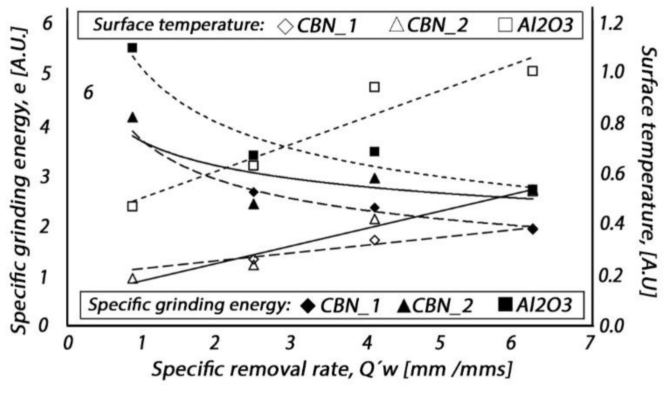

Figure 3. Specific grinding energy for Al_2O_3, CBN_1 and CBN_2. Values are relative to AISI 51200 steel. The surface temperature, T_{max}, was calculated based on eq.2 using the grinding power and process setting. The points are relative to the highest feed rate of the Al_2O_3 wheel.

X-ray diffraction (XRD) analysis showed no evidence of grinding burn, which is typically characterized by high tensile residual stresses at the surface. In the tangential direction, the CBN wheel generated a steep residual stress gradient, with approximately −600 MPa at the surface increasing to ~0 MPa at a depth of 15 µm. In contrast, the Al_2O_3 wheel produced lower surface compressive stresses (approximately −200 MPa), also approaching 0 MPa at 15 µm. In the axial direction, both wheels induced higher compressive surface stresses, approximately −900 MPa for the CBN wheel and −700 MPa for the Al_2O_3 wheel, with stresses relaxing to ~0 MPa at a depth of 15 µm. Overall, both grinding conditions resulted in compressive near-surface residual stresses that decreased with depth, with no indication of thermally induced tensile stresses.

3.2. Hard turning

Figure 4 shows the variation of thrust force (F_p) with spiral cutting length (SCL) for tool grades 1205, TH1000, and TS2000 at a cutting speed of 60 m/min. The data indicates a strong feed-dependent effect on cutting forces, tool wear, and surface integrity. At the highest feed (f = 0.15 mm/rev), F_P rise sharply over the shortest SCL (~110 m): TH1000 starts near 400 N and exceeds 600 N, accompanied by severe flank wear (VB_{max} ~ 0.35 mm). In contrast, 1205 shows a moderate increase to ~240 N with VB_{max} ~0.10 mm, while TS2000 reaches ~300 N at 110 m and VB_{max} ~0.17 mm. At the intermediate feed (f = 0.10 mm/rev), forces grow over an SCL of ~162 m: TH1000 and 1205 rise to ~375 N and 450 N, respectively, while TS2000 remains lower (~300 N) with restrained wear (VB_{max} ~ 0.17 mm). At the lowest feed (f = 0.05 mm/rev), forces increase gradually over the longest SCL (~324 m): TH1000 and 1205 reach ~375 N and 450 N, respectively, whereas TS2000 remains lowest (100 N → 300 N) with minimal wear (VB_{max} ~ 0.12 mm). Surface roughness (R_a) follows a similar trend, increasing from 0.15 to 0.59 µm for 1205 and from 0.29 to 0.60 µm for TH1000, while TS2000 shows a moderate rise (0.15 → 0.32 µm).

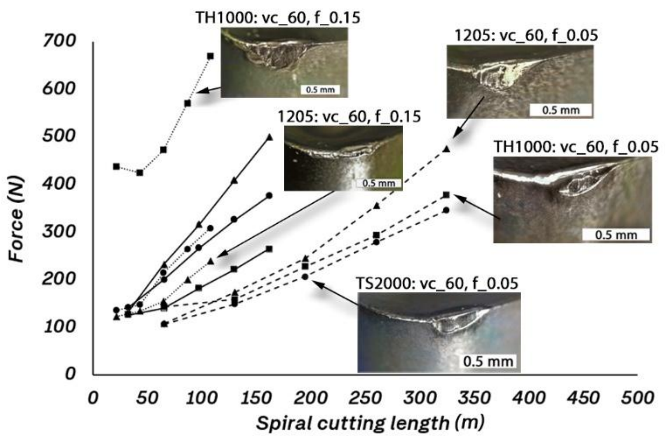

Figure 4. Measured thrust force, F_p [N], versus the spiral cutting length [m] for 1205 (▲), TH1000 (■) and TS2000 (●) inserts at v_c 60m/min and f at 0.05 (dashed line), 0.1 (solid line) and 0.15 (dotted line) mm/rev. Embedded micrographs represent some of the show the corresponding VB_{max} values for selected cutting conditions.

Table 3 shows the measured R_a and VB_{Max} for the conditions. For 1205, axial stress decreased from ~ −1613 MPa to −1075 MPa, while TH1000 and TS2000 exhibited similar relaxation, albeit with material-dependent magnitudes (Figure 5). This reduction reflects the combined effect of higher mechanical load and thermal input at elevated feeds, promoting stress redistribution and mitigating axial plastic deformation severity.

Table 3. Summary of surface roughness and tool wear results for SF1205, TS2000, and TH1000 inserts as a function of cutting speed and feed.

		Ra [µm]			VBMax [mm]		
	Cutting speed, v_c (m/min)	Feed, f (mm/rev) 0.05	0.1	0.15	Feed, f (mm/rev) 0.05	0.1	0.15
SF1205	40		0.49			0.10	
	60	0.15	0.19	0.59	0.20	0.20	0.10
	80		0.38			0.21	
TS2000	40		0.31			0.10	
	60	0.15	0.19	0.32	0.12	0.19	0.17
	80		0.24			0.26	
TH1000	40		0.85			0.11	
	60	0.29	0.59	0.60	0.18	0.12	0.35
	80		0.50			0.21	

The Full Width at Half Maximum (FWHM) of diffraction peaks, indicative of lattice strain and work hardening, showed material-specific trends. The 1205 insert displayed a clear decrease in axial FWHM with feed (8.03° → 7.34°), suggesting reduced cold work at higher feeds, likely due to thermal softening. In contrast, TH1000 and TS2000 exhibited non-monotonic changes: initial reduction followed by a slight increase at the highest feed (up to +0.45° and +0.12°, respectively), indicating localized intensification of plastic deformation rather than a systematic rise. Conditions with the highest forces and wear (e.g., TH1000 at f = 0.15 mm/rev) corresponded to elevated FWHM and relaxed compressive stresses, confirming the interplay between cutting forces, thermal–mechanical load, and surface integrity.

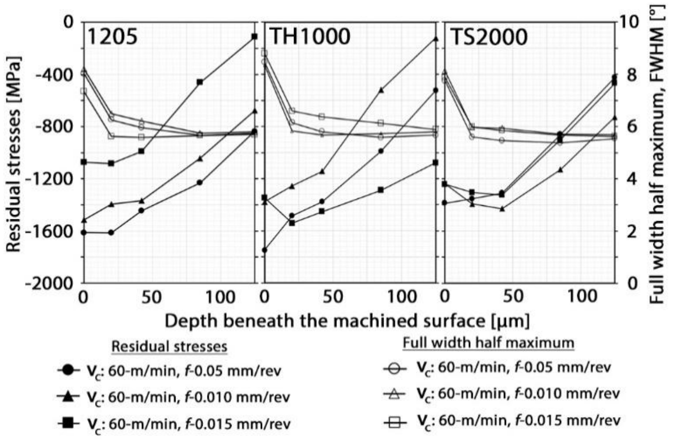

Figure 5. Axial residual stresses and axial FWHM-values as a function of depth beneath the machined surfaces after hard turning for the studied cutting tools. Errors bars omitted for clarity; uncertainties are small, ~1.5–2.5% of the values.

Microstructural observations revealed no white layer (WL) formation for TH1000 and TS2000 at 0.05 mm/rev, whereas 1205 produced a thin WL across the machined surface (Figure 6a). At 0.10 mm/rev, both 1205 and TH1000 generated WLs, and at the highest feed (Figure 6b–c), all inserts produced continuous WL coverage. For TH1000, this transition progressed from isolated WLs on feed marks to complete surface coverage (Figure 6d). The abrasive nature of Vibenite® 280 (~20 vol% carbides; high ECC) intensifies edge wear and modifies stress partitioning. This agrees with classic observations that higher carbide content and vanadium carbide morphology increase abrasive severity and reduce process efficiency, even though these effects were historically discussed in the context of grinding [13–15,16–17].

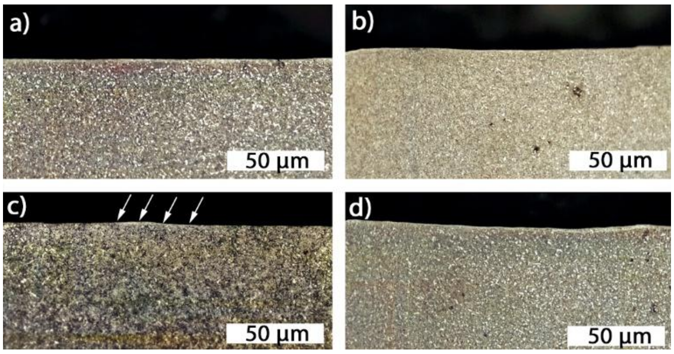

Figure 6. Observed white layers during hard turning of the Vibenite® 280. a) 1205: v_c 60 and *f* 0.05, b) 1205: v_c 60 and *f* 0.15, c) TS2000: v_c 60 and *f* 0.15, d) TH1000: v_c 60 and *f* 0.15. v_c in m/min and *f* in mm/rev.

4. Conclusions

This study examined the machinability and surface integrity of PBF-EB-produced Vibenite® 280 through grinding and hard turning. Key results show that:

1. Pre-grinding is required to correct as-printed ovality and roughness, ensuring dimensional accuracy.
2. CBN wheels clearly outperform Al_2O_3, providing stable grinding, high thermal resistance, and beneficial compressive residual stresses without burns. Using a fine-dressed general-purpose CBN wheel, Q'_w up to 6 $mm^3/mm\cdot s$, R_a ~ 0.3 µm, and a G-ratio of 100 were achieved without thermal damage.
3. Hard turning is feasible, but tool wear and surface integrity depend strongly on feed rate and insert grade. Cemented-carbide Sandvik 1205 showed the best balance, while higher feeds increased wear and reduced compressive stresses.
4. Hard-turned surfaces exhibited beneficial compressive stress profiles, including characteristic hook-shaped behavior favorable for fatigue performance.
5. The material's extreme abrasiveness, driven by its high carbide content and elevated ECC (~4× M50), remains a challenge for cost-effective finishing.

Overall, precision machining of Vibenite® 280 is achievable for high-wear, high-accuracy applications. Future work should focus on optimizing grinding parameters and thermal control to extend wheel life, and on improved tool materials, coatings, and adaptive strategies to minimize wear, white-layer formation, and surface-integrity degradation during hard turning.

Acknowledgements

Mr. R. Andersson, Mr. P. Bergagård, Mr. R. Lundstrom, Mr. J. Nordberg, N. Janebrink, Mr. C. Vårholm and Mr. H. Kurrewar at AB SKF are all greatly acknowledged for their support during the project. Mr. Anders Brage at Chalmers University of Technology is acknowledged for his help. VBN Components AB are acknowledged for providing printed rings and their support during the project.

Declaration of generative AI and AI-assisted technologies in the manuscript preparation process

The authors have used CoPilot to improve the linguistics of the manuscript, after which the authors have reviewed and edited the content, and take full responsibility of the article.

References

[1] Fischmeister HF, Riedl R. Solidification of high-speed tool steels. Metallurgical and Materials Transactions 1989;20:2133-48.
[2] A SC, Domankova M. Microstructure and properties of M2 high-speed steel cast by the gravity and vacuum investment casting. Vacuum 2019;162:183-98.
[3] Luo YW, Guo HJ, Sun XL, Guo J, Wang F. Influence of tempering time on the microstructure and mechanical properties of AISI M42 high-speed steel. Metallurgical and Materials Transactions A 2018;49:5976-86.
[4] Shen W, Yu L, Liu H. Diffusion welding of powder metallurgy high speed steel by spark plasma sintering. Journal of Materials Processing Technology 2020;275:1-9.
[5] DebRoy T, Wei HL, Zuback JS, Mukherjee T, Elmer JW, Milewski JO, et al. Additive manufacturing of metallic components – Process, structure and properties. Progress in Materials Science 2018;92:112-224.
[6] Zhong Y, Rännar L-E, Liu L, Koptyug A, Wikman S, Olsen J, et al. Additive manufacturing of 316L stainless steel by electron beam melting for nuclear fusion applications. Journal of Nuclear Materials 2017;486:234-45.
[7] Hatami S, Ma T, Vuoristo T, Bertilsson J, Lyckfeldt O. Fatigue strength of 316L stainless steel manufactured by selective laser melting. Journal of Materials Engineering and Performance 2020;29:3183-94.
[8] Liu W, Wang J, Wei Y, Zhang L, Ren Y, Han L, Yang X, Tang H, Liu S, Yang S. Electron beam melting of H13 hot-work steels: mechanical properties, microstructure evolution, precipitation behavior. *Journal of Materials Research and Technology*; 2025; Vol. 37:5283–5294.
[9] Iakovakis E, Roy M, Gee M, Matthews A. Evaluation of wear mechanisms in additive manufactured carbide-rich tool steels. Wear 2020;460-461:203449.
[10] Arumskog P, Khalid S, Beste U. Carbide size control in high-speed steels and hardmetals using electron beam powder bed fusion process parameters. Progress in Additive Manufacturing 2025;10:10901-12.
[11] Franklin D, Redegren E, Ulrisch M, Wistrand M. Guideline för bearbetning och slutförande av AM-komponenter. Available from: https://www.metalliskamaterial.se/sv/fakta/ny-guideline-for-bearbetning-av-am-komponenter/.
[12] Tarason LP. Grindability of tool steels. Transactions of the American Society of Metals 1951;43.
[13] Tarasov LP. Factors affecting the grindability of highly alloyed steels. Proceedings of the International Conference of Manufacturing Technology, ASTM 1967:689-702.
[14] Roberts GA. Vanadium high-speed steel. Transactions of the Metallurgical Society of AIME 1966;236:950-63.
[15] Kunze E, Brandis H. Einfluß der Gehalte an Carbidbildnern auf Härteannahme und Anlaßbeständigkeit beim Schnellarbeitsstahl. Deutsche Edelstahlwerke Technische Berichte 1964;4(2):75-9.
[16] König W, Messer J. Influence of carbide content on grindability of high-speed steels. Proceedings of the International Conference on Manufacturing Technology, ASTM; 1967:689–702.
[17] Badger J, Grindability of Conventionally Produced and Powder-Metallurgy High-Speed Steel, Annals of the CIRP Vol. 56/1/2007, 353-356.
[18] C. Beamer, P. Arumskog, J. Shipley, A. Magnusson, U. Beste, J. Sjöström, and M. Bergman, "Wear resistant AM components enabled with in-HIP heat treatment," Quintus Technologies, VBN Components, 2023.
[19] Ekdahl J, Dahlqvist P. Grinding behavior of high-speed steels produced by additive manufacturing. Master's thesis, Chalmers University of Technology; 2025.
[20] Rowe W B, Principles of Modern Grinding Technology, ISBN 9780815520184
[21] Shore P, Billing O, Puhasmagi V, Standard grinding wheel assessment method to support a sophisticated grinding knowledge based system, Key Engineering Materials (Vol 257-258), p 285-290.
[22] Malkin S., Guo C., Grinding Technology 2nd ed, ISBN 9780831132477